A numerical revisit of backward-facing step flow problem

T. P. Chiang and Tony W. H. Sheu[a)]
*Department of Naval Architecture and Ocean Engineering, National Taiwan University, 73 Chou-Shan Rd.,
Taipei, Taiwan, Republic of China*

In the present study we take a fresh look at a laminar flow evolving into a larger channel through a step configured in a backward-facing format. We conduct steady three-dimensional Navier–Stokes flow analysis in the channel using the step geometry and flow conditions reported by Armaly *et al.* This allows a direct comparison with the results of physical experiments, thus serving to validate the numerical results computed in the range of $100 \leqslant \mathrm{Re} \leqslant 1000$. Results show that there is generally excellent agreement between the present results and the experimental data for $\mathrm{Re} = 100$ and 389. Fair agreement for $\mathrm{Re} = 1000$ is also achieved, except in the streamwise range of $15 \leqslant x \leqslant 25$. The main difference stems from the fact that the roof eddy is not extended toward the midspan in the channel with a span width 35 times of the height of the upstream channel. In the present study we also reveal that the flow at the plane of symmetry develops into a two-dimensional-like profile only when the channel width is increased up to 100 times of the upstream step height for the case with $\mathrm{Re} = 800$. The present computational results allow the topological features of the flow to be identified using critical point theory. The insight thus gained is useful in revealing a mechanism for the development of an end-wall-induced three-dimensional vortical flow with increasing Reynolds number. © *1999 American Institute of Physics.* [S1070-6631(99)00704-7]

I. INTRODUCTION

Recirculating eddies in a flow have long been known to have a marked influence on shear stress distributions and heat transfer rates. As a subject of fundamental importance in fluid mechanics, we consider this issue by investigating a laminar flow over a backward-facing step shown schematically in Fig. 1. This configuration provides a convenient simple geometric shape for a detailed examination of the rich character of a vortical flow. In this study, we consider the step geometry and flow conditions reported by Armaly *et al.*[1] It is due to the available experimental data that this problem has become a standard numerical test and the subject of an international workshop.[2] Much two-dimensional numerical work has been done to analyze this problem. The probable reason for the lack of three-dimensional investigations is limited computer power. Advances in the last decade in parallel processing and CFD techniques have reached the point where capabilities required to conduct realistic simulations are now available. Nevertheless, there are relatively few three-dimensional studies of this problem.[3–11] There is, therefore, a strong need to carry out flow analysis in order to obtain a sufficient understanding of the three-dimensional vortical flow structure.

The experimental data of Armaly *et al.*,[1] while being often referred to, have not been rigorously confirmed through computational studies. This has prompted the current research into numerical justification of the experimental work

by conducting a full three-dimensional simulation of the Armaly *et al.* step geometry for Reynolds numbers in the range of $100 \leqslant \mathrm{Re} \leqslant 1000$. The present work is directed toward examining the span width effect on the three-dimensional expansion flow development behind the step configured in the backward-facing format.

The remaining sections of the paper are organized as follows. We first describe the governing equations and their associated boundary conditions, which are applicable to primitive-variable incompressible Navier–Stokes equations. This is followed by an introduction to the finite volume method used to discretize differential equations, the discretization scheme applied to approximate advective fluxes, and
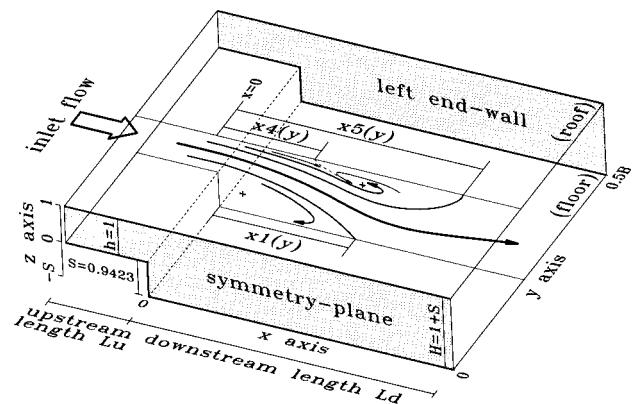

FIG. 1. Backward-facing step channel geometry and the definition of separation length x_4 and the reattachment lengths x_1 and x_5.

[a)]Corresponding author. Fax: 886-2-23929885; electronic mail: sheu@indy.na.ntu.edu.tw

862

the semi-implicit iterative solution algorithm implemented to retain velocity–pressure coupling. In the next section we provide a foundation for future studies on computed results to faithfully illuminate the flow structure. In this study, we adopt the mathematically rigorous theory of topology. Greater insight into the physical phenomena is therefore gained. In the results section, we begin by validating the computer code through an analytic test and then compare the computed results with the experimental data of Armaly et al.[1] In the present study, we vary the channel width and vary the Reynolds number to examine their effects on the flow development. Finally, we offer conclusions.

II. GOVERNING EQUATIONS AND PREDICTION METHOD

The study of vortical flows over a backward-facing step necessitates three-dimensional analysis of incompressible Navier–Stokes equations. In the absence of gravity, the governing equations for Newtonian fluid flows are studied at the steady state. These equations are cast in the following dimensionless form:

$$\frac{\partial}{\partial x_m}(u_m u_i) = -\frac{\partial p}{\partial x_i} + \frac{1}{\text{Re}^*}\frac{\partial^2 u_i}{\partial x_m \partial x_m}, \tag{1}$$

$$\frac{\partial u_i}{\partial x_i} = 0. \tag{2}$$

For comparison purposes, the Reynolds number Re^* is evaluated with a reference velocity equal to the mean velocity u_{mean} ($\equiv 1$), which is measured upstream of the step, and with a reference length equal to the upstream channel height h ($\equiv 1$). In the above elliptic equations, u_i ($i = 1-3$) refer to velocity components normalized by u_{mean}, and p is the isotropic pressure, which is normalized by ρu_{mean}^2. The independent variable, $\mathbf{x}$, is made dimensionless by h. It is noted that Re^* shown in Eq. (1) differs from the Reynolds number, $\text{Re} = u_{\text{mean}}(2h)/\nu$, defined in the work of Armaly et al.[1] The above definitions lead to $\text{Re} = 2\,\text{Re}^*$.

It has been shown that the primitive-variable equations (1)–(2) accommodate closure boundary conditions.[12] The solution is sought in a domain partly bounded by inflow–outflow boundary surfaces and partly bounded by solid walls. Upstream, we suppose that fully developed flow prevails. Therefore, we prescribe a fully developed velocity profile[13] to yield a mean velocity $u_{\text{mean}} = 1$ at the inlet plane:

$$\mathbf{u}_{\text{inlet}} = [u(y,z),0,0], \tag{3}$$

where

$$u(y,z) = \frac{48}{\alpha \pi^3}\beta(y,z), \tag{4}$$

$$\alpha = 1 - \frac{192B}{\pi^5}\sum_{i=1,3,5,\ldots}^{\infty}\frac{\tanh(\xi)}{i^5}, \tag{5}$$

$$\beta(y,z) = \sum_{i=1,3,5,\ldots}^{\infty}(-1)^{(i-1)/2}$$
$$\times\left(1 - \frac{\cosh[(2z-1)\xi]}{\cosh(\xi)}\right)\frac{\cos(2y\xi)}{i^3}, \tag{6}$$

$$\xi(i) = \frac{\pi \cdot i}{2B}. \tag{7}$$

In the above, B denotes the channel width. Far enough downstream, the flow is again fully developed at the outlet. In this study, the outlet is set $55h$ downstream from the step. At this outflow boundary, the condition describing zero gradients for field variables can be assumed. The channel is considered to be symmetric about the midplane, and this plane is taken as the solution domain. Thus, we apply symmetric boundary conditions at the midplane. At the roof and at the floor of the channel, no-slip boundary conditions are prescribed to close the problem. Here, it is significant to note that no pressure boundary conditions are required at the no-slip wall; otherwise, the differential system given by Eqs. (1)–(2) would be overdetermined.

The use of the primitive-variable formulation, while accommodating closure boundary conditions, creates a serious computational problem, since there is no representative equation for pressure. Several techniques have been proposed to overcome this difficulty, among which we consider the SIMPLE segregated formulation, which has been detailed elsewhere by Patankar.[14] The algorithm involves solv-

TABLE I. Mesh details in the numerical simulation of the backward-facing step flow problem for the $B = 35h$ case.

Grid	L_u	L_d	N_x	N_y	N_z	$\Delta x(\text{min,max})$	$\Delta y(\text{min,max})$	$\Delta z(\text{min,max})$
Grid-C	0	55	100	85	40	(0.03,1.0)	(0.03,0.25)	(0.03,0.062)
Grid-CU	−10	55	125	85	40	(0.03,1.0)	(0.03,0.25)	(0.03,0.062)
Grid-CX	0	55	150	85	40	(0.03,0.8)	(0.03,0.25)	(0.03,0.062)
Grid-CY	0	55	100	120	40	(0.03,1.0)	(0.03,0.25)	(0.03,0.062)
Grid-CZ	0	55	100	85	60	(0.03,1.0)	(0.03,0.25)	(0.016,0.046)
Williams and Baker (Ref. 9)	−1	30	91	24	20		$\Delta y_{\text{min}} = 0.167$	$\Delta z_{\text{min}} = 0.042(\text{floor})$ $\Delta z_{\text{min}} = 0.023(\text{roof})$
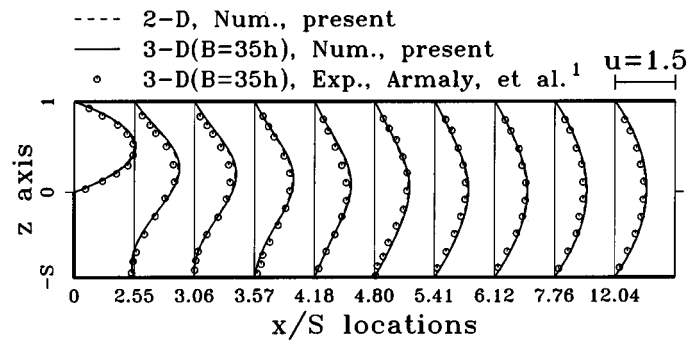
(a)
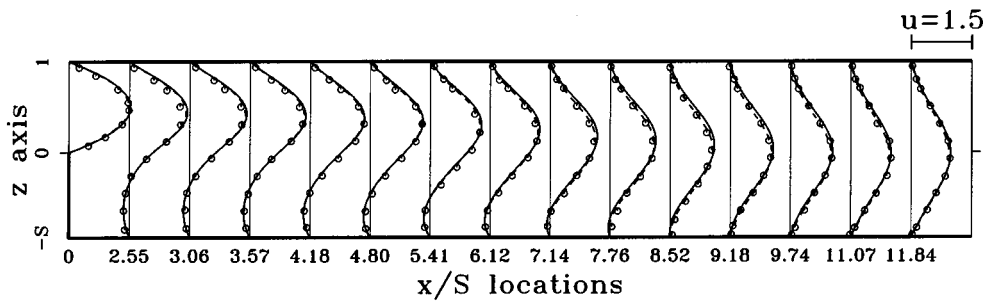
(b)
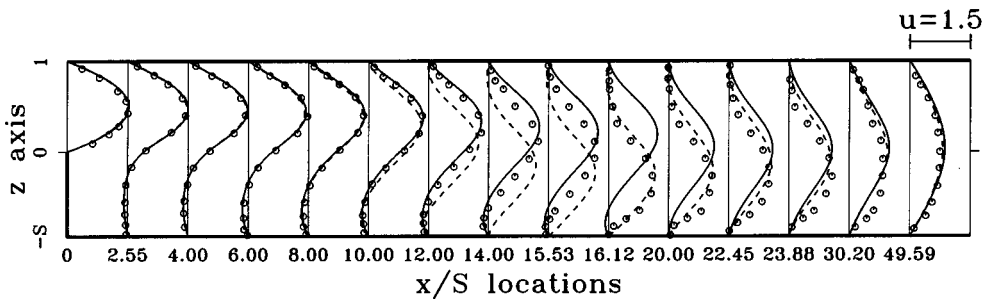
(c)

FIG. 2. Streamwise velocity profiles at the $y=0$ symmetry plane for the case of (a) Re=100; (b) Re=389; (c) Re=1000.
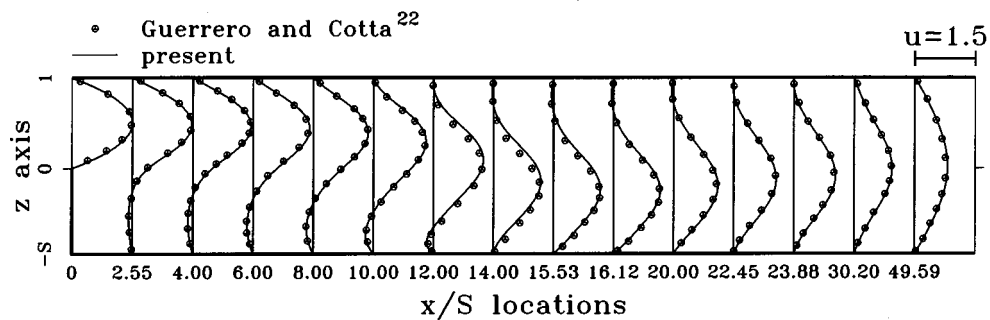

FIG. 3. A comparison of the present and the Guerrero and Cotta two-dimensional streamwise velocity profiles for the case of Re=1000.
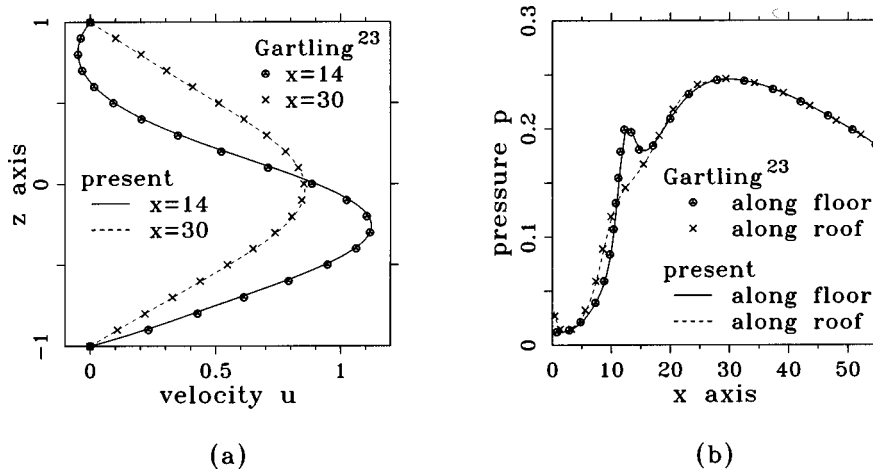
FIG. 4. A comparison of the present and Gartling's two-dimensional results for the case of Re=800. (a) Streamwise velocity profiles at $x=14$ and $x=30$; (b) the pressure distribution along the floor and the roof.

ing three momentum equations and one pressure Poisson equation by means of a cyclic prediction and correction operations. In this way, the velocities are first calculated from the momentum equations for a guessed pressure field, which is calculated, in turn; then, the velocities are adjusted such that continuity is satisfied.

It is necessary to transform the partial differential equations (1)–(2) into their algebraic counterparts so that they will be amenable to computer simulation. For this study, discretization equations are derived by integrating the governing equations over control volume cells. The main dependent variables are calculated on a staggered grid system to prevent the occurrence of pressure oscillations and avoid the requirement of pressure boundary conditions. When simulating Navier–Stokes equations, it is important to provide an accurate approximation of advective fluxes in a multidimensional domain. To this end, we adopt the second-order accurate QUICK scheme of Leonard[15] to approximate advective fluxes in the equations. The rest of the spatial derivatives are approximated by means of a second-order accurate centered difference scheme.

III. A BRIEF DESCRIPTION OF THE TOPOLOGICAL STUDY ON A THREE-DIMENSIONAL VELOCITY VECTOR FIELD

Advances in computer hardware and computational fluid dynamics in the past decade have made three-dimensional flow simulation feasible. We feel that there is a strong need to obtain a further understanding of the three-dimensional flow features that are difficult to resolve experimentally. To achieve this goal, we can conduct a topological study of

limiting streamlines[16] or skin-friction lines,[17] or visualize the density of helicity.[18] Our approach is to conduct a topological study of limiting streamlines to provide a lucid description of the fluid flow. The insight thus gained may be useful in relating the results of laboratory investigations of Armaly et al.[1]

Limiting streamlines are streamlines close to a surface. The theory behind the topology study employed here is well established (refer to Legendre[16]). The kinematic aspects of limiting streamlines are best described by singular points, such as nodes, foci, and saddle points. Limiting streamlines tend to diverge from the line of attachment. The converse of a line of attachment is a line of separation. Just as with a line of attachment, a line of separation is featured by neighboring streamlines that converge to this critical line. Through determination of these singular points, together with the lines of separation and attachment, the flow structure pertinent to the flow can be accurately depicted.

IV. RESULTS AND DISCUSSION

In numerical exploration of engineering flows, it is important to provide definite verification of the computational method by solving a problem that has an analytic solution.[19] Readers can refer to Ref. 20 for further details. This analytic verification gives us confidence that we have demonstrated the integrity of the computer code employed. Next, our attention is directed toward investigating the backward-facing step problem to further confirm the integrity of the numerical analysis.

The present study is concerned with the step geometry and Reynolds numbers reported by Armaly et al.[1] The backward-facing step has an expansion ratio $\gamma = H/h$

TABLE II. A summary of the lengths x_1, x_4, and x_5 for the case of Re $=800$ and $S=1.0$ (two-dimensional results).

2-D, Re=800, $S=1$	x_1	x_4	x_5	x_5-x_4
Gartling (Ref. 23)	12.2	9.7	20.96	11.26
Gersho et al. (Ref. 24)	12.2	9.72	20.98	11.26
Grid-C: $(\Delta x, \Delta z)$min=0.03	12.33	9.65	21.26	11.61
Test 1: $(\Delta x = \Delta z = 0.025)$	12.15	9.5	21.03	11.53
Test 2: $(\Delta x = \Delta z = 0.031)$	12.12	9.42	21.04	11.62
Test 3: $(\Delta x = \Delta z = 0.05)$	11.96	9.14	21.01	11.87

TABLE III. A summary of the lengths x_1, x_4, and x_5 for the case of Re$=1000$ and $S=0.9423$ (two-dimensional results).
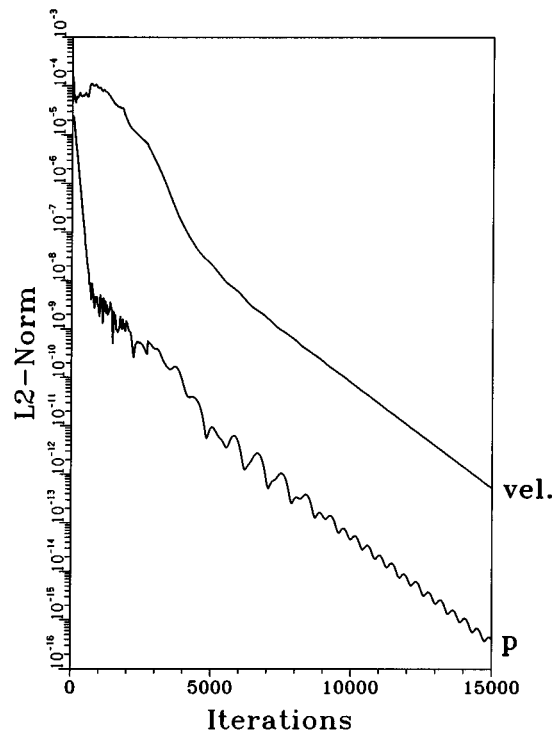
2-D, Re=1000, $S=0.9423$	x_1	x_4	x_5	x_5-x_4
Grid-C: $(\Delta x, \Delta z)$min=0.03	13.01	10.16	23.68	13.52
Test 1: $(\Delta x = \Delta z = 0.025)$	12.78	9.95	23.33	13.38
Test 2: $(\Delta x = \Delta z = 0.031)$	12.73	9.86	23.32	13.46
Test 3: $(\Delta x = \Delta z = 0.05)$	12.5	9.5	23.2	13.7
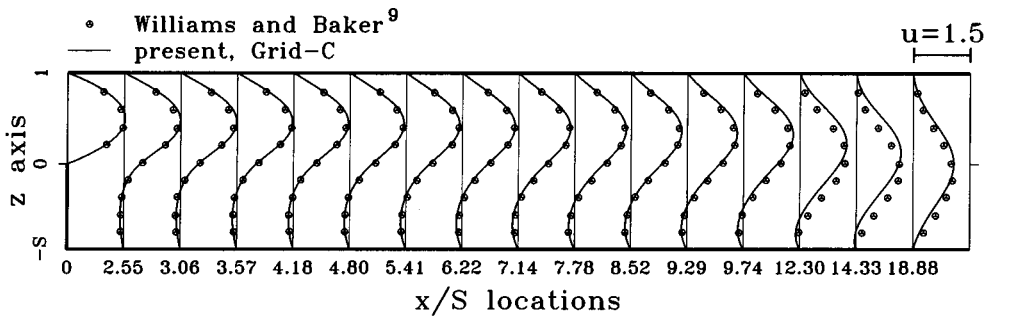
(a)
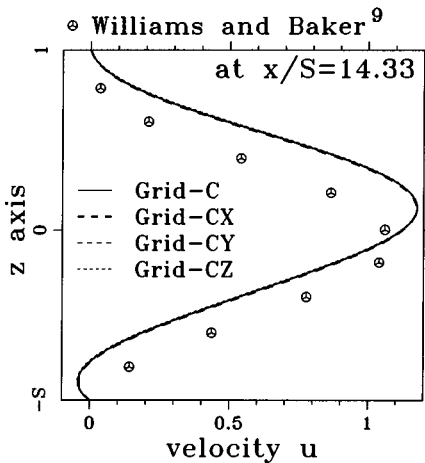
(b)

(c)

FIG. 5. The streamwise velocity profiles, computed on different grids for the case of Re=800 and $B=35h$. (a) Streamwise velocity profiles computed at the plane of symmetry using the grid Grid-C; (b) solutions computed on Grid-C, Grid-CX, Grid-CY, and Grid-CZ at $x/S=14.33$; (c) convergence history plots.

=1.9423, as shown in Fig. 1, over which the flow that develops in the upstream channel expands suddenly into a downstream channel. This allows direct comparison with the experimental results so as to further validate the numerical results and also to justify the experimental data. The Reynolds numbers considered for the verification purpose are Re=100, 389, 800, 1000 (or Re*=50, 194.5, 400, 500), and the span B of the channel has a value of $35h$ in order to mimic the experiments done by Armaly et al.[1]

There has been some debate as to the influence of the upstream channel on the flow development in the downstream channel. For a realistic simulation of Armaly's experiment,[1] we attach a straight channel with a length of 10h upstream of the step plane. At the inlet, a fully developed flow is specified according to Eqs. (3)–(7). In the analysis that considers the upstream channel as part of the solution domain, we conduct analyses in the grid Grid-CU ($L_u=-10$) and in the Grid-C ($L_u=0$). These grids are detailed in Table I. Here, L_u denotes the length of the inlet channel. Results reveal that at the symmetry plane there is a 3% difference in the x_1 length between the two calculations. This observation was also reported in the two-dimensional numerical work of Barton.[21] Therefore, it is logical to dispense with the upstream channel in our subsequent backward-facing step flow simulations, at least for Reynolds numbers below 1000.
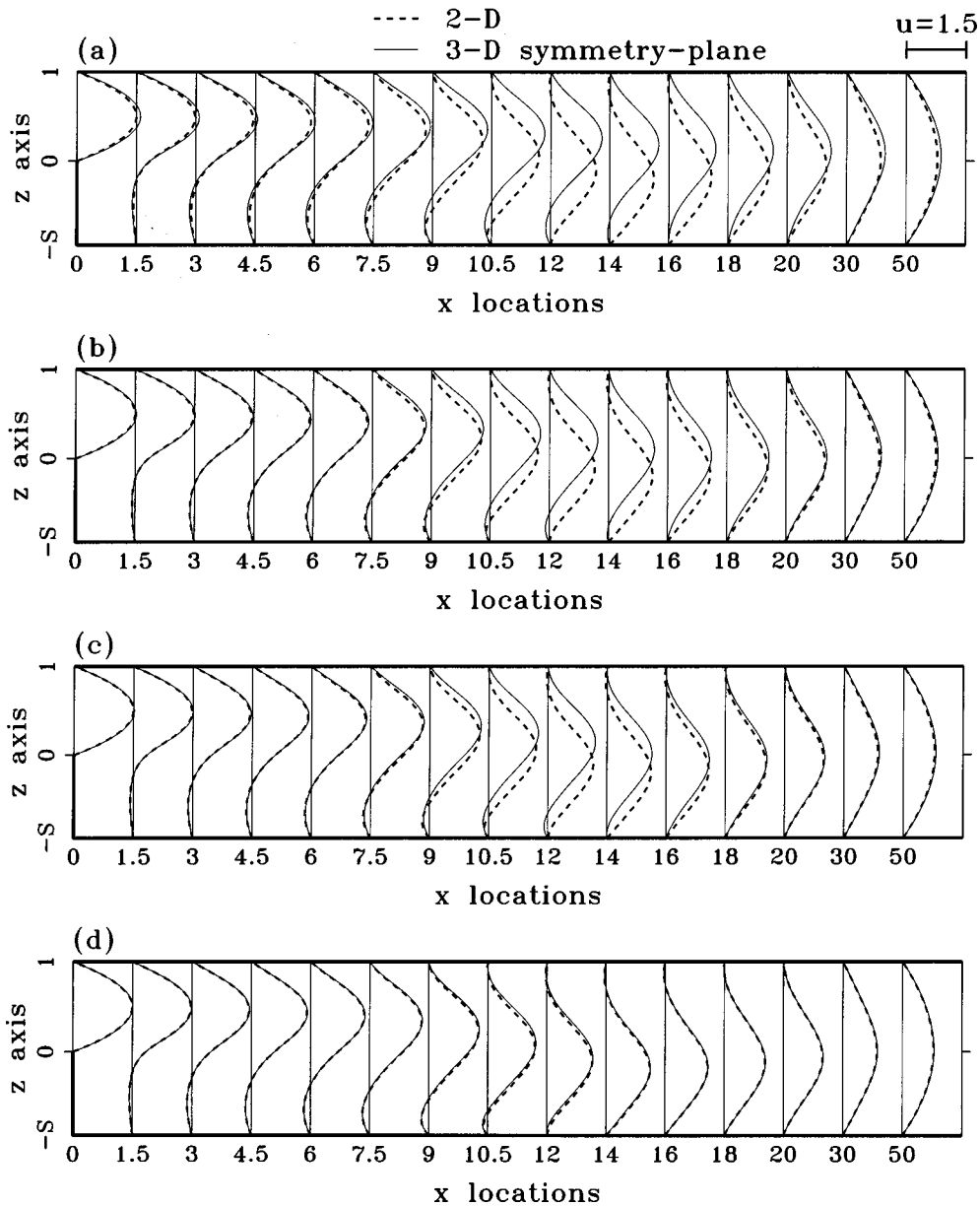
FIG. 6. The computed, together with two-dimensional results for comparative purposes, velocity profiles at the $y=0$ symmetry plane for Re=800 with different channel widths B. (a) $B=20h$; (b) $B=35h$; (c) $B=50h$; (d) $B=100h$.

It is important to note that the channel flow under investigation remains laminar for Re<1200.[1] This experimentally verified laminar flow assumption avoids complication that results from invoking turbulence modeling. We cluster grids near the vertical end wall and in the vicinity of the step plane. Gridding along the roof and floor of the channel is also crucial to resolving the eddy formation. For clarity, we summarize the grids employed in Table I for the $B=35h$ case. Results computed by Williams and Baker[9] are given in the table for the sake of comparison. The smallest and largest grid sizes in each coordinate direction are also included in Table I to aid the rational evaluation of the computed results. The length of the inlet channel, L_u, and the length of the main channel, L_d, are also shown in Table I.

A. A comparison study of computed and experimental results

In the channel with a span width $B=35h$, we present results for Re=100, 389, and 1000, which were investigated experimentally by Armaly et $al.$[1] Figures 2(a) and 2(b) show the good agreement between the measured and predicted streamwise velocities at the midplane for two cases with smaller investigated Reynolds numbers (Re=100, 389). For the case with Re=1000, evidence that there are notable differences between the three sets of results, shown in Fig. 2(c), generated interest in verifying the accuracy of the prediction.

As a first step in the verification of numerical results, we conduct a detailed comparison with other two-dimensional
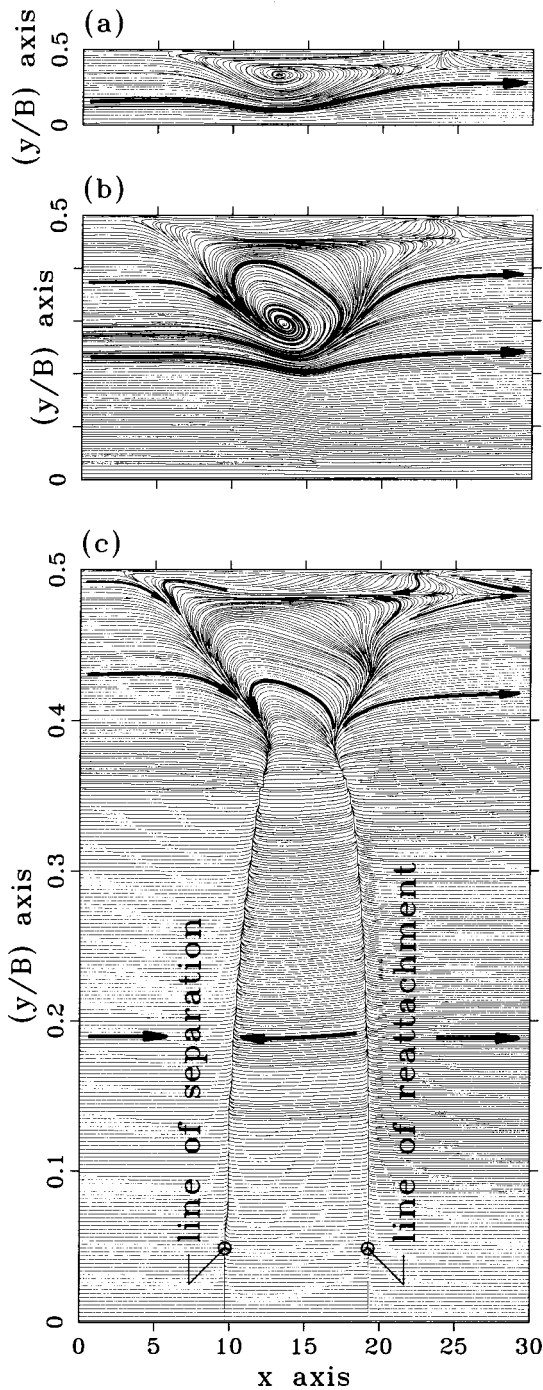
FIG. 7. Limiting streamlines on the roof of the channel for Re=800 with different channel widths B. (a) $B=10h$; (b) $B=35h$; (c) $B=100h$.

FIG. 8. Limiting streamlines on the floor of the channel for Re=800 with different channel widths B. (a) $B=10h$; (b) $B=35h$; (c) $B=100h$.

results obtained by Guerrero and Cotta[22] for Re=1000 and Gartling[23] and Gresho *et al.*[24] for Re=800 is warranted. A comparison of the streamwise velocity profiles shown in Fig. 3, the streamwise velocity profiles as well as the pressure distribution, shown in Fig. 4, and the lengths x_1, x_4, and x_5, tabulated in Tables II and III, show good agreement between the solutions. The above agreement lends additional support to the validity of the presently employed upwinding finite volume code.

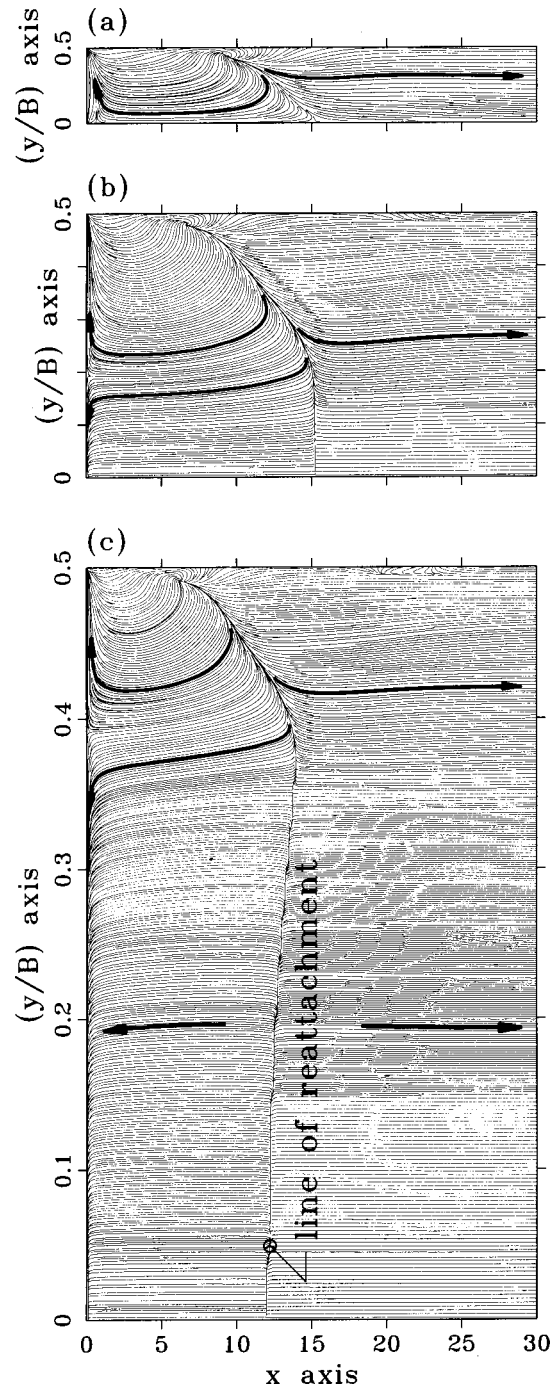We then verify our three-dimensional solutions com-

puted in Grid-C for the case with $B=35h$ and Re=800. For completeness, we also undertake a grid-refinement study by refining Grid-C to obtain Grid-CX, Grid-CY, and Grid-CZ, which are detailed in Table I. As Figs. 5(a) and 5(b)

TABLE IV. Computed reattachment length x_1/S at the symmetry plane with different widths B for Re=100, 389, and 800 ($S=0.9423$).

Re/B	2h	4h	6h	10h	20h	35h	50h	100h	$\infty(2-D)$
100	2.48	3.03	3.17	3.25		3.26			3.22
389	7.39	8.81	9.00	9.13	9.35	8.89			8.53
800	14.35	16.86	16.47	16.24	17.47	16.19	15.10	12.88	12.49

TABLE V. Computed separation length x_4/S and reattachment length x_5/S at the symmetry plane with different widths B for Re=800 and S =0.9423.

B	x_4/S	x_5/S	$(x_5-x_4)/S$
$<=35h$	None	None	None
$=50h$	12.78	19.57	6.79
$=100h$	10.19	20.68	10.49
$=\infty(2-D)$	9.78	20.69	10.91

show, the grid size we have used in this study does provide accurate solutions. We also provide evidence in Fig. 5(c) that the field solutions obtained are convergent solutions since a drop of seven to eight orders of magnitude in the residuals of the working equations is achieved.

The above two- and three-dimensional studies enlighten that in the channel with a span width $B=35h$, the end wall effect on the flow at the midplane is negligible for Re=100 and 389. This is not the case for Re=1000. To determine how wide the channel is sufficient to yield a two-dimensional-like velocity profile at the channel midspan motivates the subsequent study.

B. Span width effect on the flow development

We now investigate the effect of the channel width on the flow evolution in the channel. To this end, we fixed the Reynolds number at 800 but varied the channel widths from $B=2h$ to $4h$, $6h$, $10h$, $20h$, $35h$, $50h$, and $100h$.

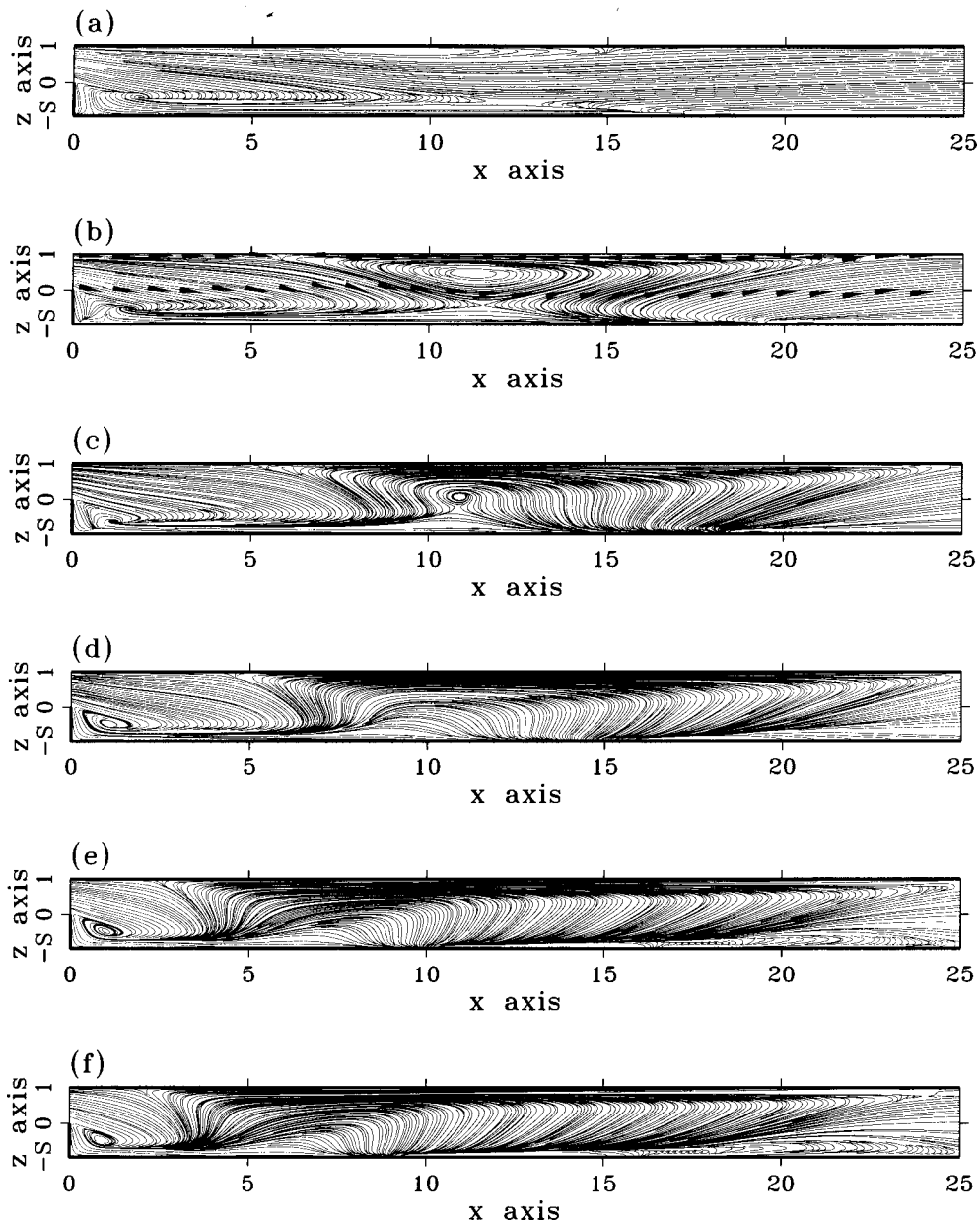Presented in Fig. 6 are computed streamwise velocity profiles at the midplane. For purposes of comparison, dotted

FIG. 9. Limiting streamlines at the vertical end wall for Re=800 with different channel widths B. (a) $B=2h$; (b) $B=4h$; (c) $B=6h$; (d) $B=10h$; (e) $B=35h$; (f) $B=100h$.

velocity profiles, obtained from two-dimensional analysis, are also plotted in each figure. What is most apparent in these figures is that the agreement between the three-dimensional solutions in the plane of symmetry and the two-dimensional solutions improves as B increases. When B reaches $100h$, the agreement can be regarded as perfect. In the middle span width range, say $B=35h$, the agreement between the two sets of data is quite good, except in the streamwise range $10 \leq x \leq 20$. This implies that the end wall effect has a negligible effect on the primary circulation in the streamwise range $x < 10$ as $B > 35h$. For velocity profiles computed under widths $B=2h$, $4h$, $6h$, and $10h$, readers can refer to Refs. 8 and 10–11 for further details.

To obtain a better understanding of the flow development, it is best to determine where the flow separates and reattaches. For this purpose, we plot limiting streamlines on the channel roof to present a detailed description of the eddy formation. Through topological studies of the velocity vector field, lines of separation and reattachment are revealed from limiting streamlines plotted in Fig. 7. We observe from the computed streamlines to find that there is evidence of an increasingly apparent developing roof eddy with the increase of the channel span. Unlike the roof eddy, which is only observed in the range of $0.3B \leq y \leq 0.5B$ for the case with $B=35h$ [Fig. 7(b)], the roof eddy extends all the way to the midplane when $B \geq 50h$. As Fig. 6(d) and Fig. 7(c) reveal, the channel width $B=100h$ is sufficient to allow the development of a two-dimensional-like velocity profile at the plane of symmetry.

We also present the limiting streamlines on the channel floor in Fig. 8 as evidence that the primary reattachment length has been captured for the eddy formed behind the step plane. One can see from Fig. 8 that limiting streamlines on the floor depart from the line of reattachment. As B increases up to $B=35h$, the largest reattachment length, x_1, is not found on the symmetry plane. At the intersection of the step plane and the channel floor, a singular point is found. This critical point is by definition a separation saddle, from which
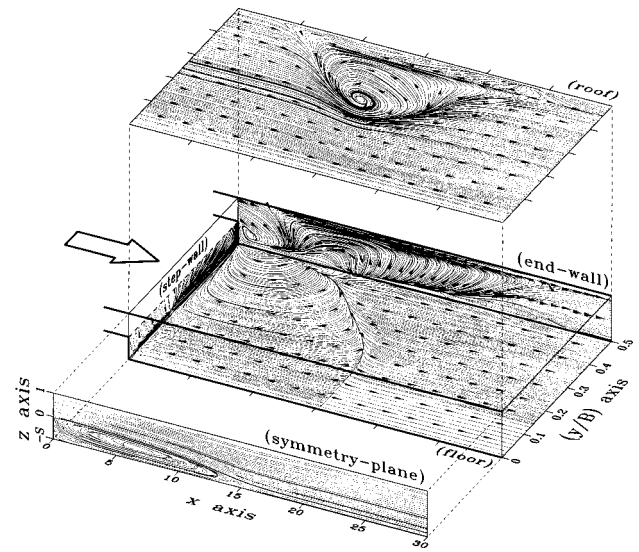

FIG. 10. Pseudostreamlines plotted on the $y=0$ symmetry plane and limiting streamlines plotted on the step, end wall, roof, and floor of the channel for the channel with $B=35h$ at Re$=800$.

streamlines repel. It is of much interest to note that for the cases of $B=35h$, $50h$, and $100h$, the distances between each critical point and the end wall are approximately the same. The y location, where $x_1(y)$, shown in Fig. 8, takes its maximum, is exactly where the distance between x_4 and x_5 reaches its minimum value on the channel roof (Fig. 7). For clarity, it is appropriate to summarize in Table IV the reattachment lengths for the primary eddy on the channel floor and in Table V the lengths of separation and reattachment of the secondary eddy on the channel roof.

We also plot in Fig. 9 limiting streamlines on the vertical end wall. In all of these figures, we can clearly observe the singular point, as configured in the foci, behind the backward-facing step. Besides the foci, we can observe another type of singular point, namely, a saddle point, in the channel with $B < 10h$ [Figs. 9(a)–9(c)]. As $B \geq 10h$, the end
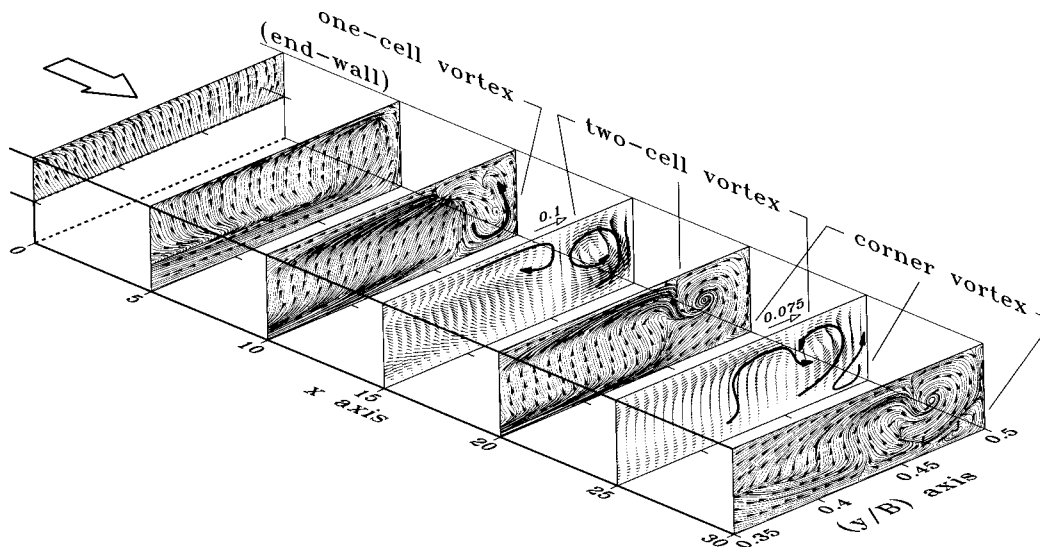

FIG. 11. The v-w pseudostreamlines and velocity vector plots at different streamwise locations showing the formation of longitudinal secondary flow near the end wall for the case of Re$=800$ and $B=35h$.

wall topologies keep changing, but they bear a similar nature. Considering the limiting streamlines plotted on the step plane, roof, floor, and end wall of the channel, it is instructive to integrate them into one figure. This helps give readers an impression of the global picture of the vortical flow structure. Due to the lack of space, we only plot in Fig. 10 the entire limiting streamlines for the case $B = 35h$.

The presentation of results is followed by plotting sectional streamlines at different x planes. The motivation is that a complete understanding of the inherent physical phenomenon cannot be achieved without observing details of the longitudinal secondary flow development downstream of the step plane. In this regard, we plot streamlines and velocity vectors at some selected transverse planes in Fig. 11 for $B = 35h$. It is found from this figure that near the end wall ($y = 0.45B - 0.5B$), the flow evolves from a single cell structure into a two-cell structure and a corner vortex. The longitudinal vortices manifest themselves near the end wall. Such a vortex motion stems from the nonlinear interaction between the primary circulation and the roof eddy. We believe that this secondary flow formation might be the cause leading to flow unsteadiness in higher Reynolds number cases.

The three-dimensional nature of the flow becomes increasingly apparent as the Reynolds number increases up to 800. Figure 12(a) plots the motion of particles originating from points near the end wall, $y = 17.5$. As to Fig. 12(b), it plots the motion of particles originating form the step plane. As the end wall topological structure shows in Fig. 12(a), particles near the end wall are entrained by primary two-dimensional motion and proceed to the midplane of the channel. It is also clearly seen from this figure that the flow has a propensity to separate from the channel roof. The three-dimensional nature of the roof separation can be more clearly seen from Fig. 12(b), in the sense that the roof eddy extends toward the midplane. Longitudinal vortices, shown in Fig. 12(c), develop and play a role in destroying the two-dimensional character of the flow. This finding was experimentally supported by Armaly et al.[1] and is consistent with the conclusion drawn by Williams and Baker.[7]

This section ends with the illumination of the y-plane flow structure in order to illustrate the role of the end wall on the formation of the roof eddy. We plot limiting streamlines close to the end wall and other selected sectional streamlines in Fig. 13 for the case with Re=800 in the channel having a span width $B = 35h$. An important feature of this plot is the complex surface streaking pattern. Particularly striking in the limiting streamlines is the presence of upward particle motion originating from the channel floor. The spiraling vortex motion has its origin in the end wall boundary layer. Fluid particles near the end wall have been entrained into the singular point situated behind the step plane. It is this flow entrainment that causes the flow to develop in the third dimension. The global three-dimensional nature of the flow is best illustrated by the vortical core line shown schematically in Fig. 13. For particles around this line they move spirally toward the plane of symmetry. Evidence indicating the probable mechanism leading to the roof eddy is also illustrated in streamlines plotted in between $0.44B \leqslant y \leqslant 0.5B$.
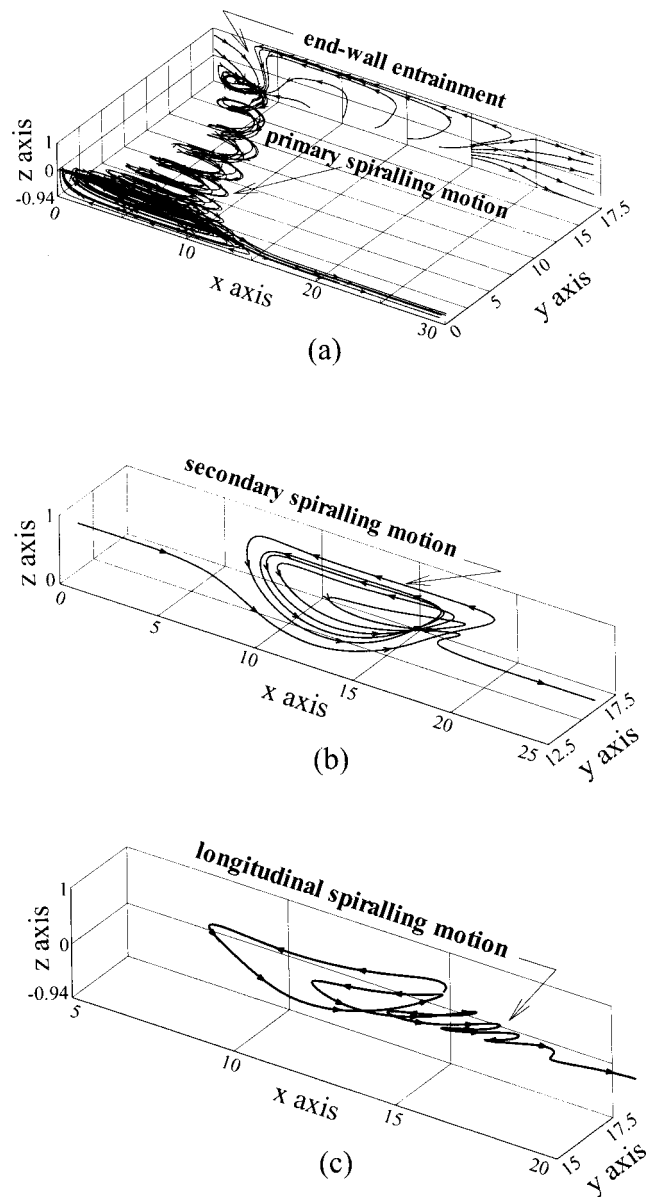

FIG. 12. An illustration showing the end-wall-induced spiral motion in the channel for the case of Re=800 and $B = 35h$. (a) End wall flow entrainment; (b) spiraling motion due to the presence of a secondary eddy on the channel roof; (c) spiraling motion for the longitudinal vortex.

C. Reynolds number effect on the flow development

When modeling one flow inside a channel, it is often desirable to change the flow conditions and then study how these changes affect the flow characteristics. It was one of the objectives of the current study to investigate the effect of the Reynolds number. The results presented were obtained for $100 \leqslant Re \leqslant 1000$ and $B = 35h$. As noted earlier, the grid size and uniformity are the same for all four investigated Reynolds numbers.

Figure 14 presents the reattachment length x_1 against y/B for $B = 35h$ and for Re=100, 389, 800, and 1000. For comparison purposes, the primary reattachment lengths x_1 for Re=100, 389, 800, and 1000 obtained from the two-dimensional analysis are also included. The dashed line plotted in this figure is physically important, in that the larger y_2
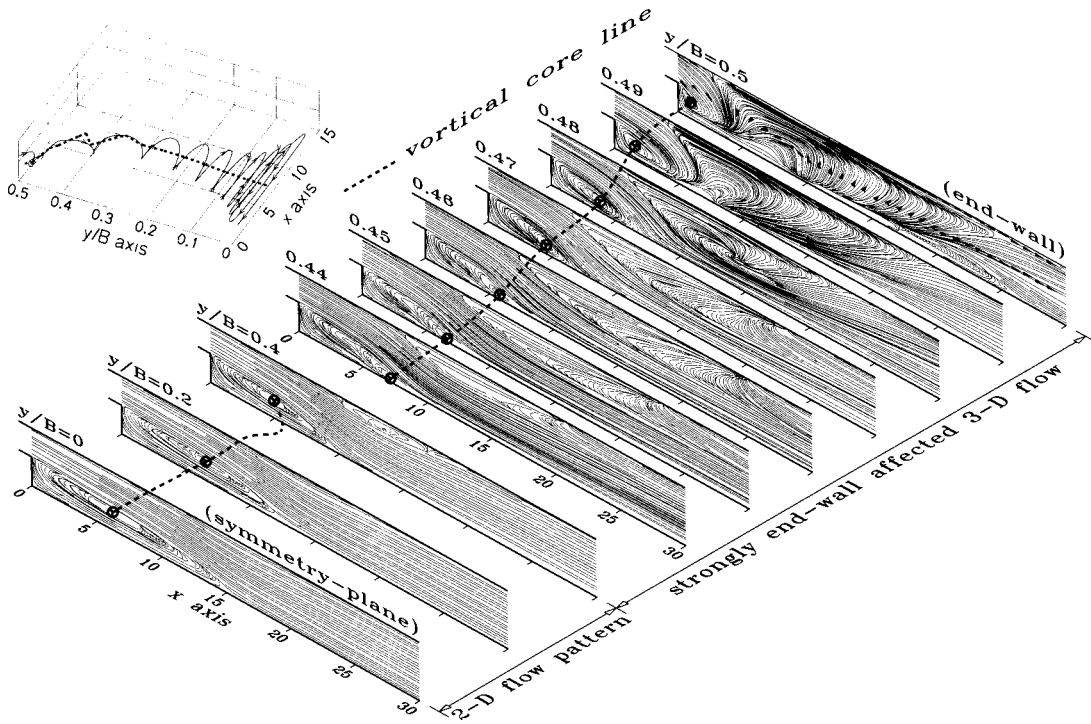
FIG. 13. Streamline plots at selected y planes to illustrate the flow structure in the channel with $B=35h$ and the flow with Re=800.
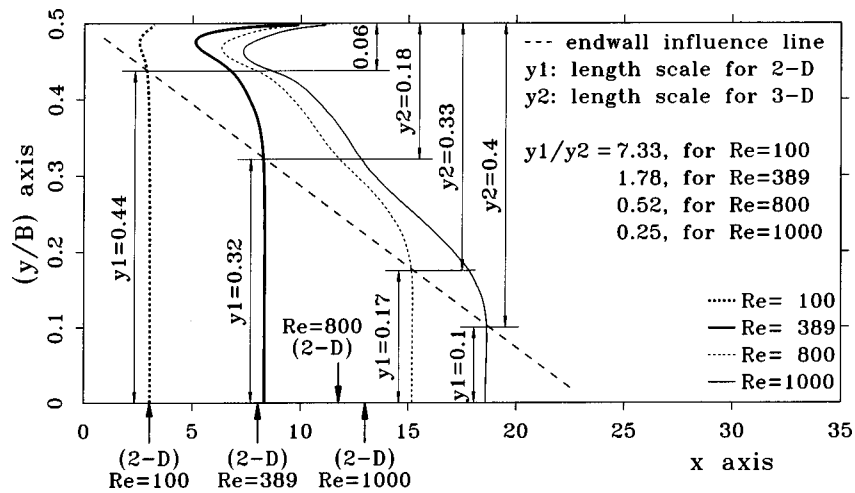

FIG. 14. The plot of length x_1 against y for the Reynolds numbers 100, 389, 800, and 1000 in the channel with $B=35h$.
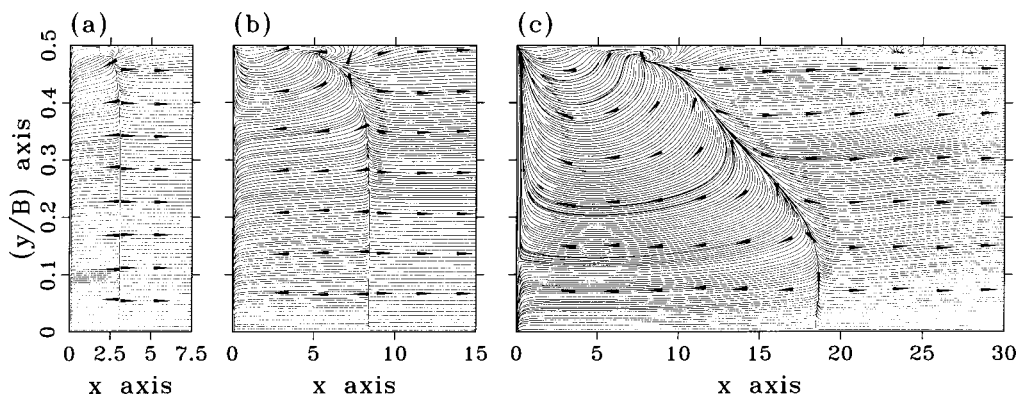

FIG. 15. An illustration showing the reattachment length x_1 for the primary separation eddy on the floor from the limiting streamline plots in a channel of width $B=35h$. (a) Re=100; (b) Re=389; (c) Re=1000.
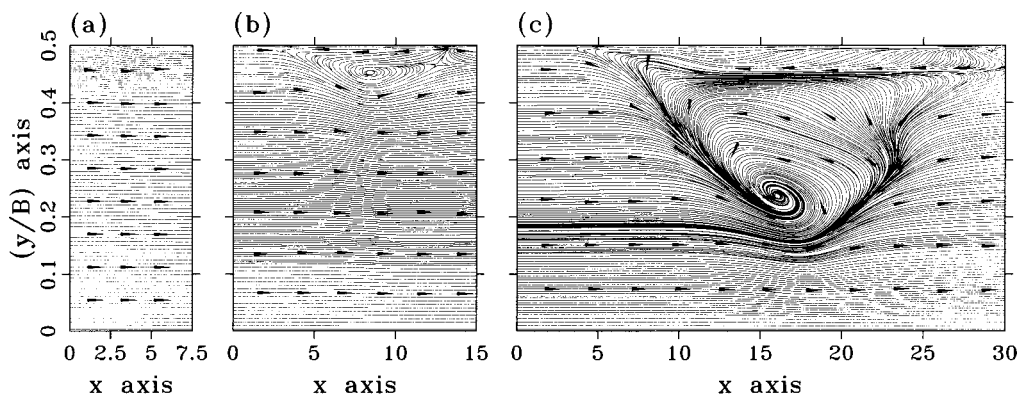
FIG. 16. An illustration showing the separation of a secondary eddy on the roof from the limiting streamline plots in a channel of width $B = 35h$. (a) Re=100; (b) Re=389; (c) Re=1000.

is, the greater is the extent to which the channel flow is affected by the end wall. As the Reynolds number increases, the ratio of y_1/y_2 decreases accordingly, in the sense that $y_1/y_2 \sim 7$, 2, $\frac{1}{2}$, and $\frac{1}{4}$ for Re=100, 389, 800, and 1000, respectively. Figure 14 provides additional evidence that on the midplane of the channel, the flow is prevailingly two dimensional for small Reynolds number cases (Re=100, 389), in that the x_1 lengths take the same values obtained based on two- or three-dimensional calculations. In contrast, the three-dimensional effect plays an essential role as the Reynolds number increases up to 800 and 1000. There exists quite a large discrepancy in the x_1 value computed within two-dimensional (2D) and three-dimensional (3D) frameworks. This finding agrees with Armaly *et al.*[1] that as Re >400 the flow was found to be strongly three dimensional. We also determine the lengths x_4 and x_5 against y by a similar means to show that even for higher Reynolds numbers, say Re=800 and 1000, the roof eddy is never observed on the midplane. This is in contradiction to the two-dimensional analysis, which shows that a roof eddy appears at a Reynolds number of 450. The direct consequence of the separation-free roof eddy on the symmetry plane in our three-dimensional analysis is that the x_1 length is greater.

Finally, we plot limiting streamlines at the floor and roof in Fig. 15 and Fig. 16, respectively. When the Reynolds number is as small as 100, the flow is predominantly two dimensional, in the sense that x_1 is invariant with y, except in the intermediate vicinity of the end wall, as shown in Fig. 15(a). The secondary separation bubble is not observed at such a low Reynolds number case [Fig. 16(a)]. At Re=389, the flow near the end wall $(0.4B \leqslant y \leqslant 0.5B)$ has a three-dimensional character [Fig. 15(b)]. As seen in Fig. 16(b), the roof separation bubble becomes clearly visible only in the limited spanwise range. Figure 16(c) shows that the separation bubble extends into the channel and terminates roughly at the spatial location where x_1 ceases to be uniform as a function of y [Fig. 15(c)].

V. CONCLUSION

A numerical investigation of laminar flow over a three-dimensional backward-facing step has been presented here

for Reynolds numbers in the range of $100 \leqslant \mathrm{Re} \leqslant 1000$. This allows a direct comparison with detailed experimental data given by Armaly *et al.*[1] The same step geometry and flow conditions were prescribed, thus enabling the validation of the numerical results and justification of the use of our developed computer code. Additionally, we considered the effect of the span width on the flow reversal and have investigated the effect of the end wall on the overall flow structure. Considerable effort has been expended in exploring the flow structure by means of a theoretically rigorous topology theory. We show that the computed surface streaking patterns give a good indication of the extent of the reverse-flow zone without resorting to oil streaking experimental study.

ACKNOWLEDGMENTS

[1] B. F. Armaly, F. Durst, J. C. F. Pereira, and B. Schönung, ''Experimental and theoretical investigation of backward-facing step flow,'' J. Fluid Mech. **127**, 473 (1983).

[2] K. Morgan, J. Periaux, and X. Thomasset, in *Analysis of Laminar Flow Over a Backward-Facing Step*, A GAMM-Workshop (Frieder Viewwy & Sohn, Germany, 1984).

[3] D. Kwak and J. L. C. Chang, ''A three-dimensional incompressible Navier–Stokes flow solver,'' Part 1-2 NS3D code, CFD workshop, University of Tennessee Space Institute, Tullahoma, TN, 1985.

[4] H. C. Ku, R. S. Hirsh, T. D. Taylor, and A. P. Rosenberg, ''A pseudospectral matrix element method for solution of three-dimensional incompressible flows and its parallel implementation,'' J. Comput. Phys. **83**, 260 (1989).

[5] T. Ikohagi, B. R. Shin, and H. Daiguji, ''Application of an implicit time-marching scheme to a three-dimensional incompressible flow problem in curvilinear coordinate systems,'' Comput. Fluids **21**, 163 (1992).

[6] B. Jiang, L. Hou, and T. Lin, ''Least-squares finite element solutions for three-dimensional backward-facing step flow,'' NASA-TM 106353, 1993.

[7] P. T. Williams and A. J. Baker, ''Incompressible computational fluids dynamics and the continuity constraint method for the three-dimensional Navier-Stokes equations,'' Numer. Heat Transfer, Part B **29**, 137 (1996).

[8] T. W. H. Sheu, T. P. Chiang, and S. F. Tsai, ''Vortical structures in channel flows with backward-facing step,'' Int. J. Turbo Jet-Engines **13**, 277 (1996).

[9] P. T. Williams and A. J. Baker, ''Numerical simulations of laminar flow over a 3D backward-facing step,'' Int. J. Numer. Methods Fluids **24**, 1159 (1997).

[10] T. P. Chiang, T. W. H. Sheu, and S. F. Tsai, ''Topological flow structures in backward-facing step channels,'' Comput. Fluids **26**, 321 (1997).

[11] T. P. Chiang and T. W. H. Sheu, ''Vortical flow over a 3D backward-facing step,'' Numer. Heat Transfer, Part A **31**, 167 (1997).

[12] O. Ladyzhenskaza, *The Mathematical Theory of Viscous Incompressible Flow* (Gordon and Breach, New York, 1969).

[13] F. M. White, *Viscous Fluid Flow*, 2nd ed. (McGraw-Hill, New York, 1991).

[14] S. V. Patankar, *Numerical Heat Transfer and Fluid Flow* (Hemisphere New York, 1980).

[15] B. P. Leonard, ''A stable and accurate convective modeling procedure based on quadratic upstream interpolation,'' Comput. Methods Appl. Mech. Eng. **19**, 59 (1979).

[16] R. Legendre, ''Sèparation de courant lècoulement laminaire tridimensionnel,'' Rech. Aerosp. **54**, 3 (1956).

[17] M. Lighthill, ''Attachment and separation in three-dimensional flow,'' in *Laminar Boundary Layers*, edited by L. Rosenhead (Oxford University Press, Oxford, 1963), Vol. II.

[18] Y. Levy, D. Degani, and A. Seginer, ''Graphical visualization of vortical flows by means of helicity,'' AIAA J. **29**, 1347 (1990).

[19] C. R. Ethier and D. A. Steinman, ''Exact Fully 3D Navier–Stokes solutions for benchmarking,'' Int. J. Numer. Methods Fluids **19**, 369 (1994).

[20] T. P. Chiang, R. R. Hwang, and W. H. Sheu, ''Finite volume analysis of spiral motion in a rectangular lid-driven cavity,'' Int. J. Numer. Methods Fluids **23**, 325 (1996).

[21] I. E. Barton, ''The entrance effect of laminar flow over a backward-facing step geometry,'' Int. J. Numer. Methods Fluids **25**, 633 (1997).

[22] J. S. Perez Guerrero and R. M. Cotta, ''Benchmark integral transform results for flow over a backward-facing step,'' Comput. Fluids **25**, 527 (1996).

[23] D. K. Gartling, ''A test problem for outflow boundary conditions—Flow over a backward-facing step,'' Int. J. Numer. Methods Fluids **11**, 953 (1990).

[24] P. M. Gresho, D. K. Gartling, J. R. Torczynski, K. A. Cliffe, K. H. Winters, T. J. Garratt, A. Spence, and J. W. Goodrich, ''Is the steady viscous incompressible two-dimensional flow over a backward-facing step at Re =800 stable?,'' Int. J. Numer. Methods Fluids **17**, 501 (1993).